Electronic Supplementary Information

Exceptional Performance of Hierarchical Ni-Fe Oxyhydroxide@NiFe Alloy Nanowire Array Electrocatalysts for Large Current Density Water Splitting

Caiwu Liang,[a] Peichao Zou,[a] Adeela Nairan,[a] Yongqi Zhang,[b] Jiaxing Liu,[a] Kangwei Liu,[a] Shengyu Hu,[a] Feiyu Kang,[a] Hong Jin Fan,*[b] Cheng Yang*[a]

a.Division of Energy and Environment, Shenzhen International Graduate School, Tsinghua University, Shenzhen 518055, China;

b.School of Physical and Mathematical Sciences, Nanyang Technological University, 21 Nanyang Link, 637371, Singapore;

Email: yang.cheng@sz.tsinghua.edu.cn

Email: fanhj@ntu.edu.sg

Experiment methods

Fabrication of Ni_xFe_{1-x}-AHNAs

The Ni_xFe_{1-x}-AHNAs was fabricated by a one-step chemical deposition process. A commercial nickel foam (thickness:1.5mm, bulk density: 0.19 g cm^{-3}) was employed as the substrate. All solutions in the experiments were prepared with analytical grade chemicals and deionized water. Before chemical deposition, the nickel foam was sonicated in 2M HCl solution for 20 min to remove the NiO_x surface layer, and subsequently rinsed with water and acetone, then allowed to dry in air. After that the Ni_xFe_{1-x} nanowires were in situ deposited onto this nickel foam using a modified method analogous to one of our recent works.[1] Typically for $Ni_{0.8}Fe_{0.2}$-AHNA, a 30 mL aqueous solution (defined as solution A) containing 0.066 M $NiCl_2$, 0.033 M $FeCl_2$, 37.5 mM $Na_3C_6H_5O_7$ (sodium citrate) and 0.53 mM H_2PtCl_6 was prepared, plus another aqueous solution (defined as solution B) containing 8.5 vol% of hydrazine hydrate. Then, the above nickel foam was placed inside a beaker vertical to the magnetic field created by electromagnet (East Changing Technologies, Inc). Prior to the reaction, the pH value of the solution A and B was adjusted to 12.5 with 6 M KOH aqueous solution at room temperature measured by a pH meter (HORIBA, F-71), respectively. The Then solution A and solution B were heated to 80 ℃ separately followed by mixing them together in a water bath. The reactions involved in the synthesis of Ni_xFe_{1-x}-AHNA can be expressed as follows:

$$N_2H_4 + 4OH^- \rightarrow N_2 + H_2O + 4e^- \quad (1)$$

$$N_2H_4 + OH^- \rightarrow N_2 + NH_3 + H_2O + e^- \quad (2)$$

$$Ni\ (II) + 2e^- \rightarrow Ni \quad (3)$$

$$Fe\ (II) + 2e^- \rightarrow Fe \quad (4)$$

At the initial stage, Ni (II) and Fe (II) are rapidly reduced into numerous nanoparticles

by hydrazine hydrate, where Ni (II) (or Fe (II)) represents all the Ni (II) (or Fe (II)) species, such as Ni^{2+}, $NiOH^{+}$, $Ni(OH)_2$, $HNiO_2^{-}$, and NiO_2^{2-}.[2] These nanoparticles are deposited onto the nickel foam under a strong magnetic force owing to the ferromagnetic properties of metallic Ni_xFe_{1-x} nanoparticles. Since the direction of magnetic domain in the NiFe particles are consistent with the magnetic field, the nanoparticles will repel each other in the direction parallel to the substrate; as a result, the as-formed nanoparticles are more likely to be deposited on the existing particles with same magnetic domain direction and grow into nanowire instead of growing densely all over the nickel foam surface without the gap. After 60 min's reaction, Ni_xFe_{1-x}-AHNAs could be deposited onto the nickel foam. Finally, the Ni_xFe_{1-x}-AHNA samples were washed for three times with deionized water and ethanol, and then dried in a desiccator at 60 ℃ for 2h. The average mass loading of the as-obtained $Ni_{0.8}Fe_{0.2}$-AHNA was about 2.5 mg cm^{-2}.

Fabrication of nickel nanowire arrays

The preparation process of bare Ni nanowire array was similar to that of Ni_xFe_{1-x}-AHNA, except for the precursor recipe. For Ni nanowire array, solution A was change to a 30 mL aqueous solution containing 0.1 M $NiCl_2$, 37.5 mM $Na_3C_6H_5O_7$ (sodium citrate) and 0.53 mM H_2PtCl_6, the other solutions and processes are the same as the fabrication of Ni_xFe_{1-x}-AHNAs. The average mass loading of the as-obtained Ni nanowire arrays was about 4.9 mg cm^{-2}. Notably, the very small amount of H_2PtCl_6 is used as nucleating agent to promote the formation of initial Ni seeds.[2] Therefore, Pt is theoretically only present in the most inner part of the nanoparticle and will not be exposed to the electrolyte during HER. In order to exclude the existence of Pt on the surface, we used XPS to analyze the surface composition, and no obvious Pt metal signal was detected on the Ni nanowire surface (Fig. S21).

Fabrication of IrO_2/NF electrodes

To prepare the IrO_2/NF electrodes, 40 mg IrO_2, 60 μL Nafion, 540 μL ethanol and 400 μL deionized water were ultrasonicated for 60 min to obtain a homogeneous dispersion. Then, a piece of clean nickel foam was dipped into the dispersion, which was then dried in air at 60 ℃ for 4 h. The mass loading of IrO_2 catalyst on nickel foam was controlled to be ~ 2.4 mg cm^{-2}, just close to that of $Ni_{0.8}Fe_{0.2}$-AHNA.

Fabrication of Pt/C/NF electrodes

To prepare the Pt/C/NF electrodes, 20 mg commercial Pt/C, 30 μL Nafion, 200 μL ethanol and 770 μL deionized water were ultrasonicated for 60 min to obtain a homogeneous dispersion. Then, a piece of clean nickel foam was dipped into the dispersion, which was then dried in air at 60 ℃ for 4 h. The mass loading of Pt/C catalyst on nickel foam was controlled to be ~ 2.0 mg cm^{-2}.

Materials characterization

The morphology of catalysts was characterized by field emission scanning electron microscopy (FE-SEM, SAPPHIRE SUPRA 55) and TEM (FEI-G2 Spirit, Germany,

working voltage 300 kV). Both the fresh samples and samples after OER for 24 hours at 100 mA cm^{-2} were characterized. Crystallographic information was obtained with X-ray diffraction (Bruker DSRINT2000/PC, Germany) using Cu Kα radiation with λ=1.5418 Å (at a diffraction angle ranging from 5° to 85° at a scan rate of 5°/min). The nanowire powders were directly characterized without nickel foam substrate. The Raman spectra of the materials were obtained with a spectrometer (LabRAM HR spectrometer, Horiba) operating with argon ion laser (532 nm) as the excitation light source. The X-ray photoelectron spectra (XPS) were measured with Al-Kα radiation (50 W, 15 kV) (ESCALABSB 250 Xi). An argon ion beam etching process was employed at an accelerating voltage of 2.0 kV. The BET results were obtained with an automated adsorption device (Micromeritics ASAP 2020) at 77 K. The contact angles of gas bubbles under electrolyte were tested by the method of captive bubble using Kruss DSA30 system. The volume of the measured bubble was taken around 2.5 μL. The images of oxygen bubbles release were obtained by camera (SONY NEX6) equipped with a macro lens.

Electrochemical measurement

Electrochemical measurements were conducted with electrochemical working station (CHI 660E) in a three-electrode electrochemical setup. A 1 M KOH solution was used as electrolyte, and an Ag/AgCl electrode (in 3 M KCl) and graphite rod (with a diameter of 8 mm) were used as reference and counter electrodes, respectively. The as-prepared electrodes supported on Ni foam were utilized as the working electrode. The working area was tailored to 0.25 cm^2. To convert the measured potential versus the Ag/AgCl electrode into the potential versus reversible hydrogen electrode (RHE), the Ag/AgCl reference electrode was calibrated using RHE in 1 M KOH solution. The RHE was constructed according to the previous work reported by Boettcher and co-workers.[3] Briefly, two Pt electrodes were first polished and cycled in 0.5 M H_2SO_4 electrolyte at about $\pm$ 1.8 V for 2 hours to remove the surface impurity, and then employed as both working electrode (WE) and counter electrode (CE) in 1 M KOH electrolyte. The electrolyte was saturated by hydrogen before use, and continuous H_2 was bubbled over the WE during the calibration. To perform the calibration, a series of CV measurements were carried out to determine the zero current potential (the interconversion between the hydrogen oxidation and hydrogen evolution reaction). The scan rate of the CV measurement is set as low as 0.1 mV s^{-1} to avoid the possible contribution of capacitive current. As shown in Fig. S22, the result shows that the potential of zero net current can be estimated at −1.012 V versus the Ag/AgCl electrode, and the relation between the Ag/AgCl reference and RHE in 1 M KOH solution can thus be established using formula $E_{RHE} = E_{Ag/AgCl} + 1.012$ V in 1 M KOH solution. Thus, the OER overpotential is calculated by the formula: $E_{overpotential} = E_{RHE} - 1.23V = E_{Ag/AgCl} - 0.218V$. The iR compensation was performed by automatic current interrupt method with a value of 95% × Ru through the CH instrument 660E working station. For OER, in order to provide reliable electrochemical data and avoid overlap between Ni^{2+}/Ni^{3+} oxidation and OER, polarization curves were recorded from high initial potentials to low final potentials with a 5 mV s^{-1} scan rate. HER polarization curves were characterized at a

scan rate of 1 mV s^{-1}. Tafel slopes were calculated using the polarization curves by plotting overpotential against log (current density). Chronopotentiometry measurements were performed to evaluate the long-term stability. The ECSA was determined by measuring the capacitive current associated with double-layer charging from the scan-rate dependence of CVs. For this, the potential window of CVs was 0–0.1V versus Ag/AgCl. The scan rates were 20, 40, 80, 160, 240, 320 and 400 mV s^{-1}. The double-layer capacitance (C_{dl}) was estimated by plotting the $\Delta J = (J_a - J_C)$ at 0.05V versus Ag/AgCl against the scan rate. The linear slope is twice of the double-layer capacitance C_{dl}. The ECSA values were calculated from the measured double layer capacitance divided by the specific capacitance of an atomically smooth material (C_{dl}', ~40 μF cm^{-2}): ECSA = $C_{dl} \div C_{dl}' \times$ S, where S is the actual surface area of the electrode.[4] The electrochemical impedance spectroscopies (EIS) measurement was conducted at 1.53 V and -0.15 V (vs. RHE), in the frequency range of 100 kHz to 0.1 Hz with an amplitude of 5 mV. The oxygen and hydrogen were collected using water displacement method during the water splitting electrolyzer test ($Ni_{0.8}Fe_{0.2}$-AHNA as anode and Ni nanowire array as cathode), and then the Faradaic Efficiency was calculated for both OER and HER. The evolved oxygen and hydrogen gas on the electrode were separately collected with a 50 mL graduated cylinder, which was filled with electrolyte. Constant-current electrolysis was carried out at a current density of 500 mA cm^{-2} under standard conditions (25 °C, 1 atm) for totally 50 min. During test, we recorded the volume of collected oxygen and hydrogen gas every 5 min. The accumulated charge passing through the working electrode were calculated by the equation: Q=It, where I is the electrolysis current and t is the electrolysis time.

Calculation

The most common working current density of 500 mA cm^{-2} in industrial alkaline water electrolysis is chosen for calculation. The Faradaic efficiency (FE) for our catalysts is determined to be approximately 100% for both HER and OER process (Fig. S20, ESI), and the Faradaic Efficiency of nickel/stainless pair is assumed to be as high as 100%. When 1 Kg H_2 is generated, the required amount of charge (Q) is:

$$Q = \frac{1000g \times N_A \times 2e}{M_{H_2} \times FE} = \frac{1000 \times 2 \times 6.022 \times 10^{23} \times 1.602 \times 10^{-19}}{2.016 \times 100\%} = 95706785.7\ C$$

Where N_A is Avogadro constant, e is the charge of an electron and M_{H_2} is the relative molecular mass of hydrogen.

For our electrolyzer, the cell voltage (U_1) at a current density of 500 mA cm^{-2} is 1.702 V. The amount of electricity (W_1) required to generate 1 Kg H_2 is:

$W_1 = QU_1 = 95706785.7 \times 1.702 = 162892949.3\ J \approx 45.25\ KW \cdot h$

For nickel/stainless steel electrolyzer, the cell voltage (U_2) at a current density of 500 mA cm^{-2}. The amount of electricity (W_2) required to generate 1 Kg H_2 is:

$W_2 = QU_2 = 95603174.6 \times 2.122 = 203089799.0\ J \approx 56.41\ KW \cdot h$

Therefore, the saved energy (E_{save}) per kilogram H_2 is:

$$E_{save} = W_2 - W_1 = 56.41 - 45.25 = 11.16\ KW \cdot h$$

Figures

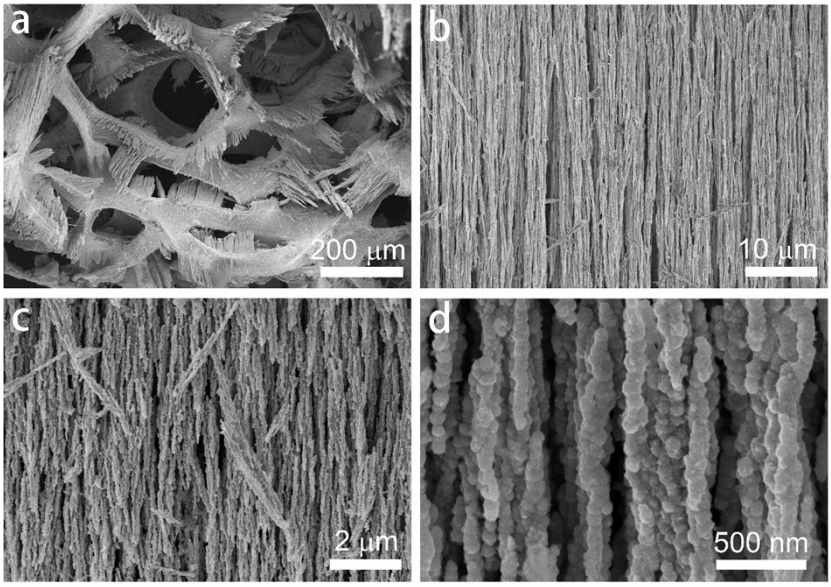

Supplementary Figure 1. SEM images of $Ni_{0.8}Fe_{0.2}$-AHNA at different magnification.

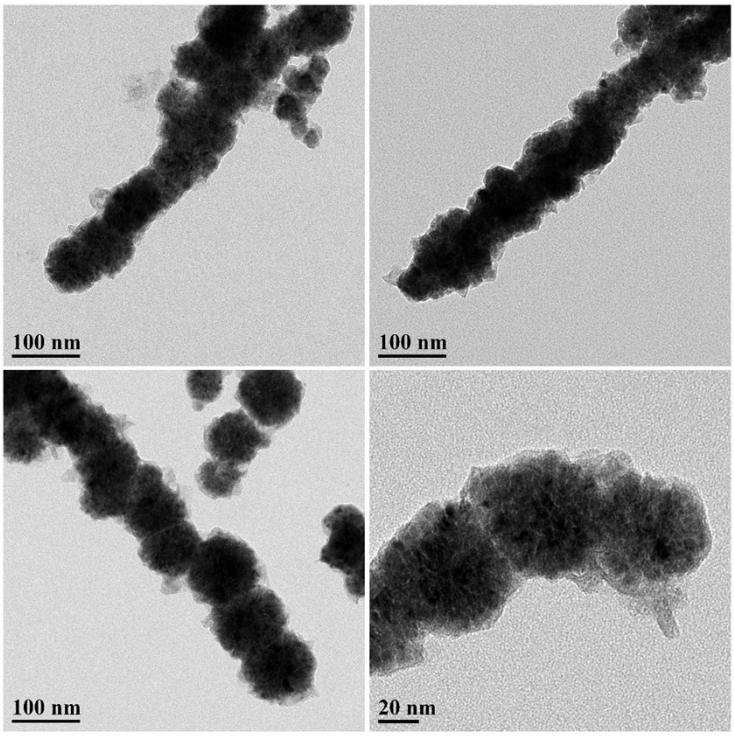

Supplementary Figure 2. TEM images of $Ni_{0.8}Fe_{0.2}$-AHNA.

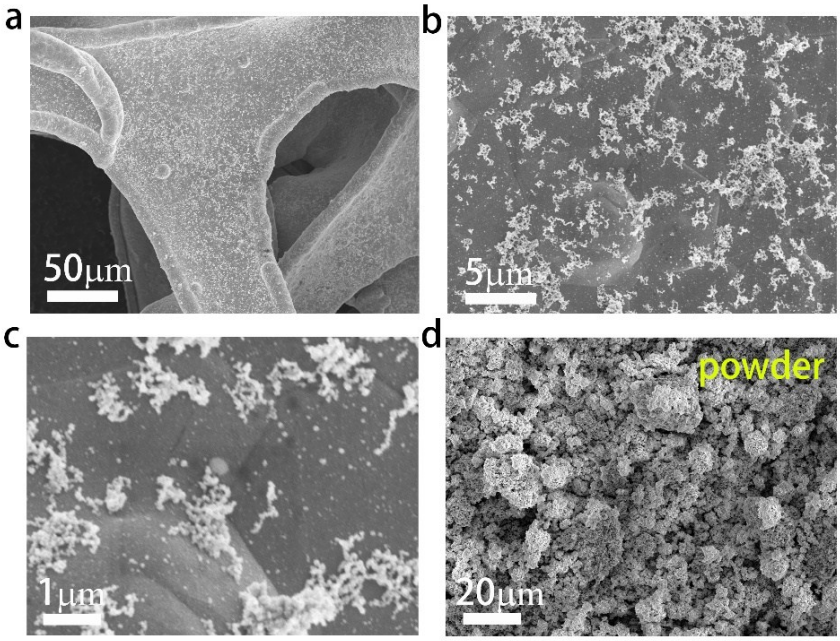

Supplementary Figure 3. Morphology of NiFe alloy without magnetic field, showing agglomerated nanoparticles (a-c) SEM images of NiFe alloy on nickel foam substrate at different magnifications. (d) SEM image of NiFe alloy powder collected from the dispersed products.

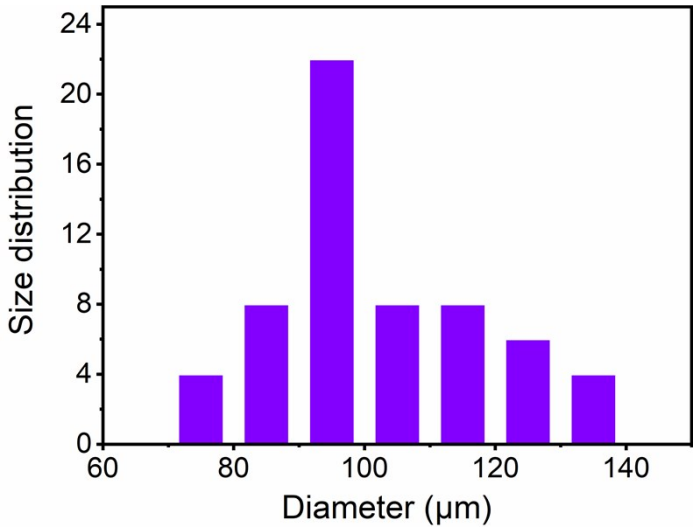

Supplementary Figure 4. Distribution of $Ni_{0.8}Fe_{0.2}$ nanowire diameter (counted from SEM image).

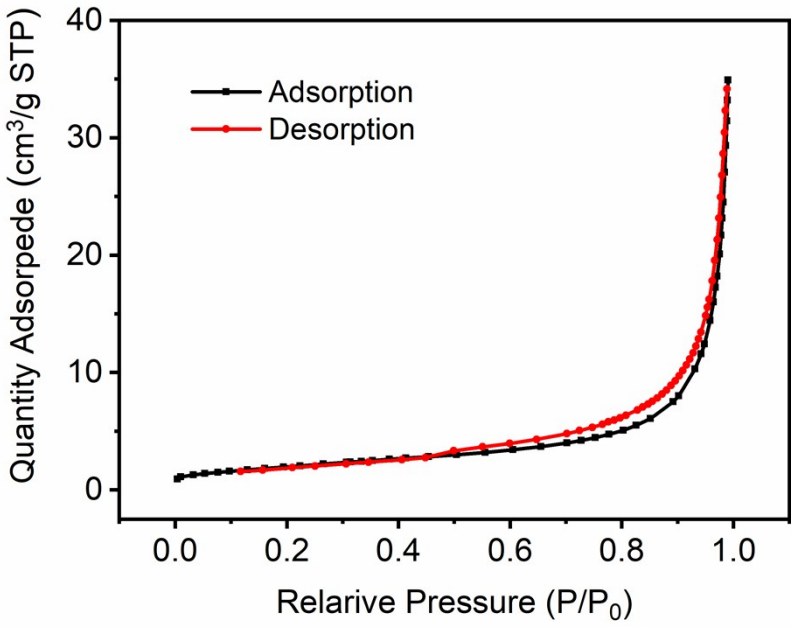

Supplementary Figure 5. BET results of $Ni_{0.8}Fe_{0.2}$-AHNA.

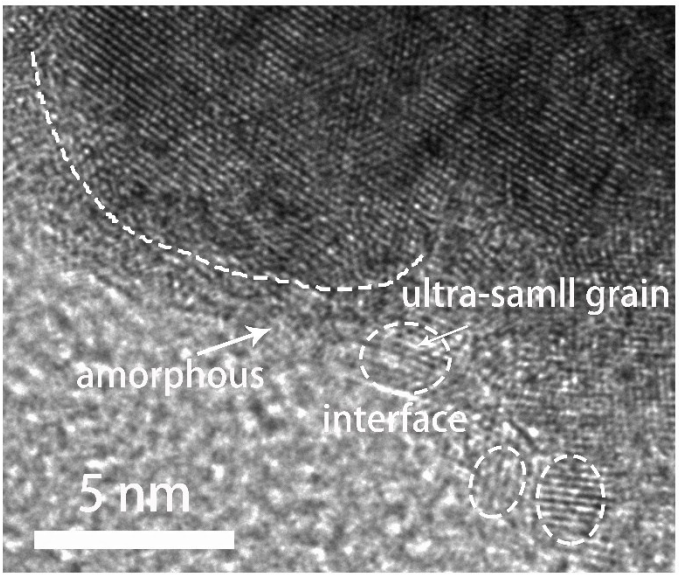

Supplementary Figure 6. HRTEM of NiFe oxyhydroxide on the surface, showing boundary between ultra-small crystalline domains and amorphous domains.

Supplementary Table 1. Ni and Fe content determined by ICP-MS.

Ni/Fe ratio in precursor	Ni content ppm（mg/Kg)	Fe content ppm（mg/Kg)	Ni/Fe ratio
8 : 1	768494	97041	7.5 : 1
5 : 1	703764	120295	5.6 : 1
3 : 1	722847	149492	4.6 : 1
2 : 1	783166	179983	4.1 : 1
1 : 1.5	601365	269719	2.1 : 1
1 : 3	517228	317614	1.6 : 1

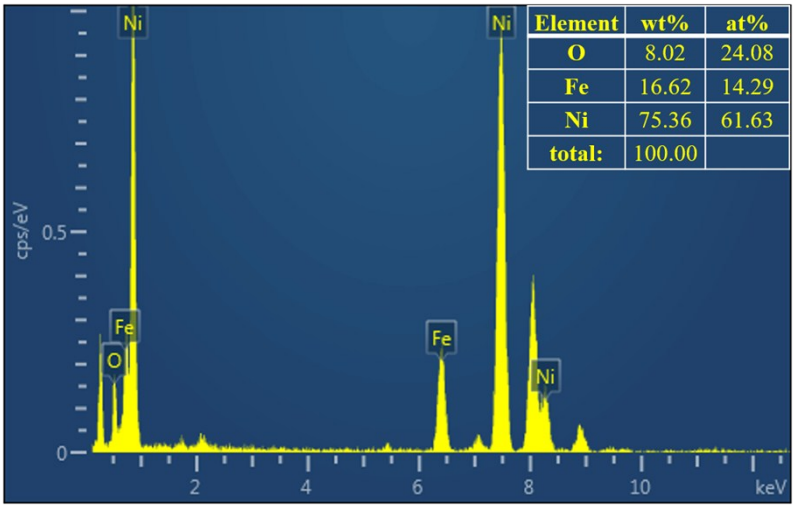

Supplementary Figure 7. EDX spectra and the corresponding Ni/Fe ratio.

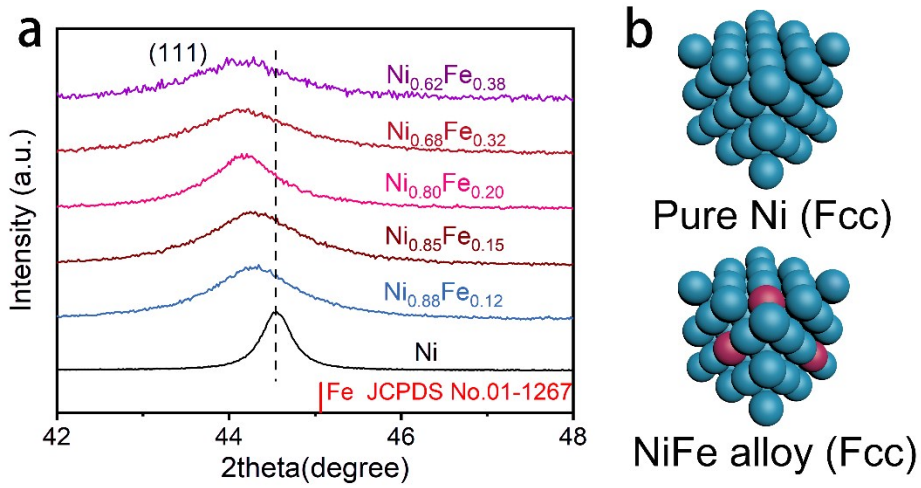

Supplementary Figure 8. (a) Enlarged XRD pattern of 2θ from 42° to 48° for pure Ni, pure Fe and different Ni_xFe_{1-x}-AHNAs, showing the diffraction peaks shift toward lower diffraction degrees with the increase of Fe content. (b) Crystal structure of pure Ni and NiFe alloy.

Supplementary Table 2. Comparison of the catalytic OER performance between our $Ni_{0.8}Fe_{0.2}$-AHNA catalyst and robust earth-abundant electrocatalysts reported in 1 M KOH. V_{20} and η_{260} correspond to the overpotential at current density of 20 mA cm^{-2} and the output current densities at the overpotential of 260 mV respectively.

OER catalysts	Support	Mass loading (mg)	V_{20} (mV)	η_{260} (mA cm^{-2})	Tafel slope (mV dec^{-1})	Reference
$Ni_{0.8}Fe_{0.2}$-AHNA	Ni foam	2.5	200	1078	34.7	Our work
$NixFe_{3-x}O_4$/Ni	GCE	0.5	250*	50*	44	ACS Energy Letters, 2018, 3(7): 1698-1707.
Se-(NiCo)S_x/$(OH)_x$ Nanosheets	Ni foam	NA	170*	120*	33.9	Adv. Mater., 2018, 30(12): 1705538.
Ni-Fe-OH@Ni_3S_2	Ni foam	NA	235*	40*	93	Adv. Mater., 2017, 29(22): 1700404.

Core–Shell Ni-Co Nanowire	Carbon fiber	0.3	310*	5*	43.6	Adv. Energy Mater., 2017, 7(1): 1601492.
Ni-Fe-O mesoporous nanowire	Ni foam	5.4	285*	15*	39	Adv. Energy Mater., 2018, 8(5): 1701347.
Co-B/Ni	Ni foil	2.4	265*	25*	68	Adv. Energy Mater., 2018, 8(26): 1801372.
Ni_3FeN-NPs	Ni foam	0.2	NA	NA	46	Adv. Energy Mater., 2016, 6(10): 1502585.
NiCoP/CNF	GCE	NA	280*	8*	83	Adv. Energy Mater., 2018, 8(20): 1800555.
FeOOH/Co/FeOOH Hybrid Nanotube Arrays	Ni foam	0.5	250*	65*	32	Angew. Chem. Int. Ed.,2016, 55(11): 3694-3698.
Ni/Fe (oxy)hydroxide nanorod arrays	Ni foam	4	NA	500*	NA	Energy Environ. Sci., 2018, 11(10): 2858-2864.
NiFe LDH/Cu nanowire arrays	Cu foam	2.2	220	100*	27.8	Energy Environ. Sci., 2017, 10(8): 1820-1827.
Core–Shell NiFeCu	Ni foam	10.2±0.5	180*	300*	33	Nat. Commun., 2018, 9(1): 381.
Iron fluoride-oxide nanoporous film	Fe foil	0.2	275*	17*	45	Nat. Commun., 2018, 9(1): 1809.
Fe@NiFe LDH	Fe foam	2.78	285*	100*	48.3	Nat. Commun., 2018, 9(1): 2609.
NiFe LDH/CNTs	Carbon paper	0.25	235*	35*	31	J. Am. Chem. Soc., 2013, 135(23): 8452-8455.
Ni_2P nanoparticles	GCE	0.14	305*	5*	NA	Energy Environ. Sci., 2015, 8(8): 2347-2351.
NiFe hydroxides	Ni foam	NA	243*	40*	28	Nat. Commun., 2015, 6(1): 6616.
FeCoNi-hybrid nanotube arrays	Ni foam	NA	NA	40*	49.9	Nat. Commun., 2018, 9(1): 2452.

*** The value is calculated from the curves shown in the literature.**

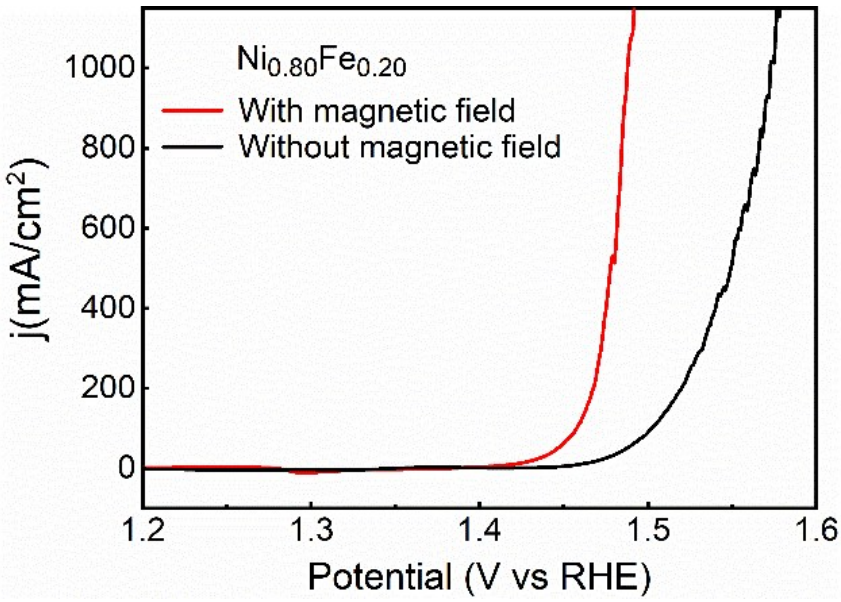

Supplementary Figure 9. The polarization curves of $Ni_{0.8}Fe_{0.2}$ alloy fabricated with and without assistance of magnetic field.

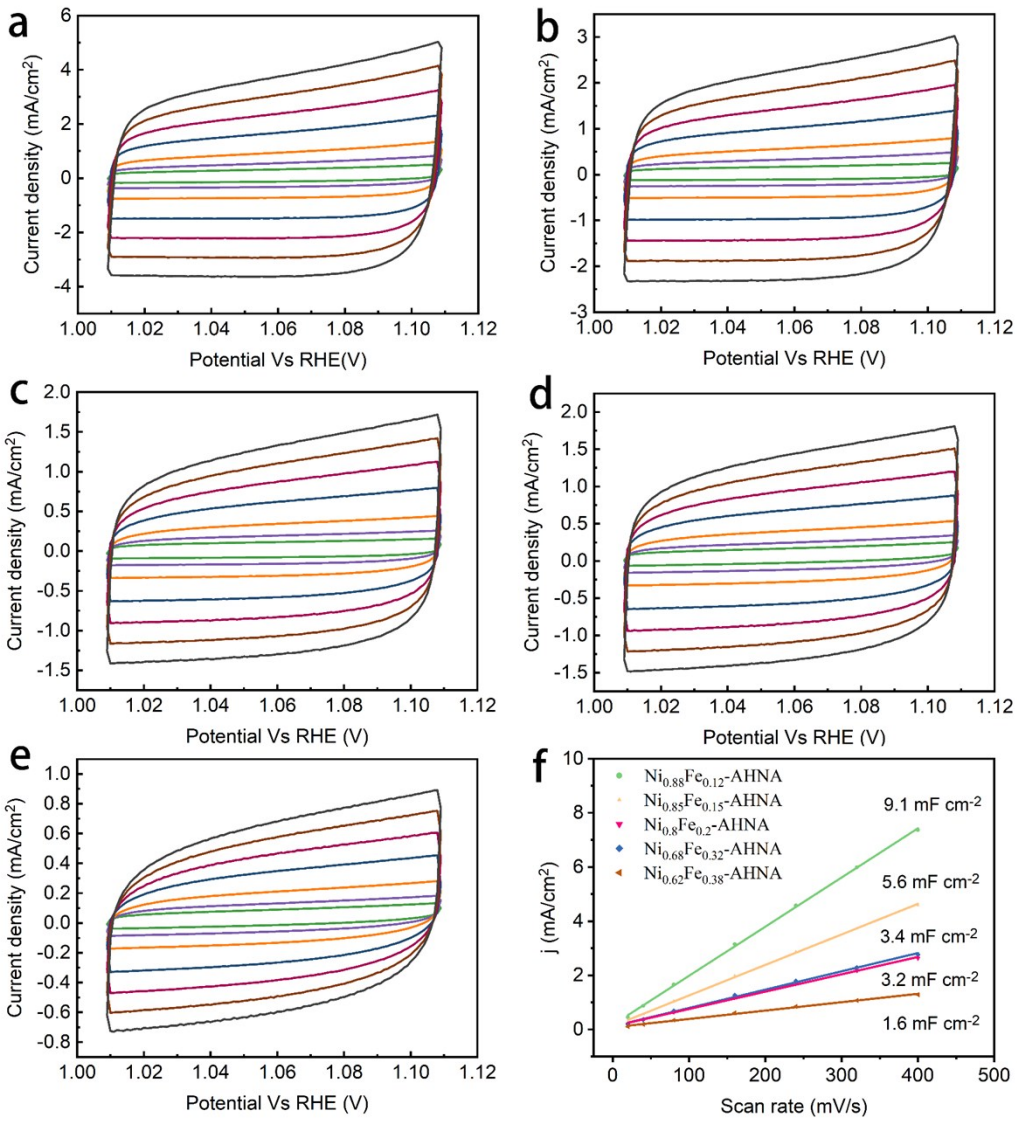

Supplementary Figure 10. CV curves at different scan rates of Ni_xFe_{1-x}-AHNAs and the corresponding $C_{dl.}$ (a) $Ni_{0.88}Fe_{0.12}$-AHNA (b) $Ni_{0.85}Fe_{0.15}$-AHNA (c) $Ni_{0.80}Fe_{0.20}$-AHNA (d) $Ni_{0.68}Fe_{0.32}$-AHNA (e) $Ni_{0.62}Fe_{0.38}$-AHNA (f) C_{dl} of different Ni/Fe ratios Ni_xFe_{1-x}-AHNAs.

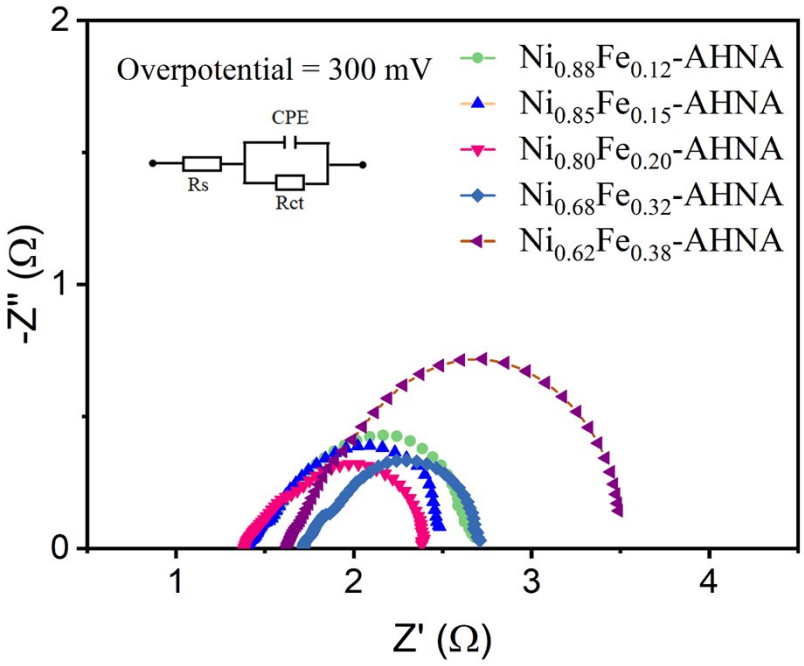

Supplementary Figure 11. EIS Nyquist plots of different Ni/Fe ratios Ni_xFe_{1-x}-AHNAs at the overpotential of 300mV.

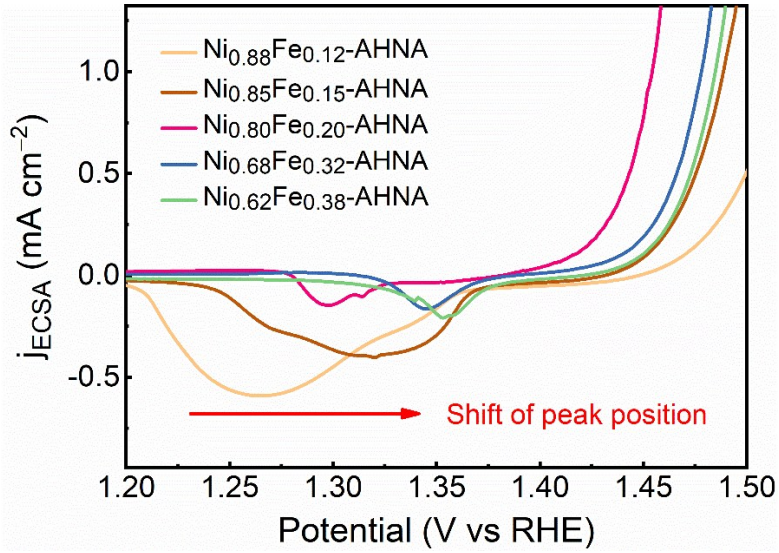

Supplementary Figure 12. Enlarged LSV curves of NiFe alloy nanowire arrays with different Ni/Fe ratios, showing the anodic shift of the Ni redox waves with increasing Fe content in NiFe oxyhydroxide.

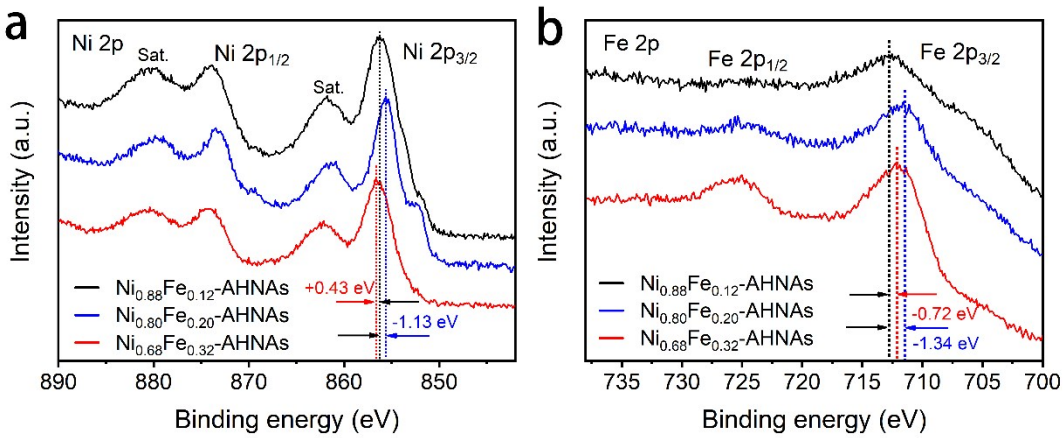

Supplementary Figure 13. (a) Ni 2p XPS spectra of $Ni_{0.88}Fe_{0.12}$-AHNA, $Ni_{0.80}Fe_{0.20}$-AHNA and $Ni_{0.68}Fe_{0.32}$-AHNA. (b) Fe 2p XPS spectra of $Ni_{0.88}Fe_{0.12}$-AHNA, $Ni_{0.80}Fe_{0.20}$-AHNA and $Ni_{0.68}Fe_{0.32}$-AHNA.

Supplementary Table 3. Comparison of intrinsic catalytic activity of $Ni_{0.8}Fe_{0.2}$-AHNA with some representative oxygen evolution electrocatalysts that have been recently reported.

Electrocatalysts	Substrate	Normalized method	Overpotential j=10mA cm^{-2} (mV)	Reference
$Ni_{0.8}Fe_{0.2}$-AHNA	Nickel foam	ECSA	255	This work
Boronized NiFe	NiFe sheet	ECSA	309	Ref. 5
IrOx/SrIrO3	SrTiO3	AFM	270	Ref. 6
NiFe(b)	GCE	ECSA	340	Ref. 7
NiCo(b)	GCE	ECSA	420	Ref. 7
IrO_x	GCE	ECSA	320	Ref. 4
Ru(a)	GCE	ECSA	290	Ref. 7
$NiCuO_x$	GCE	ECSA	410	Ref. 4

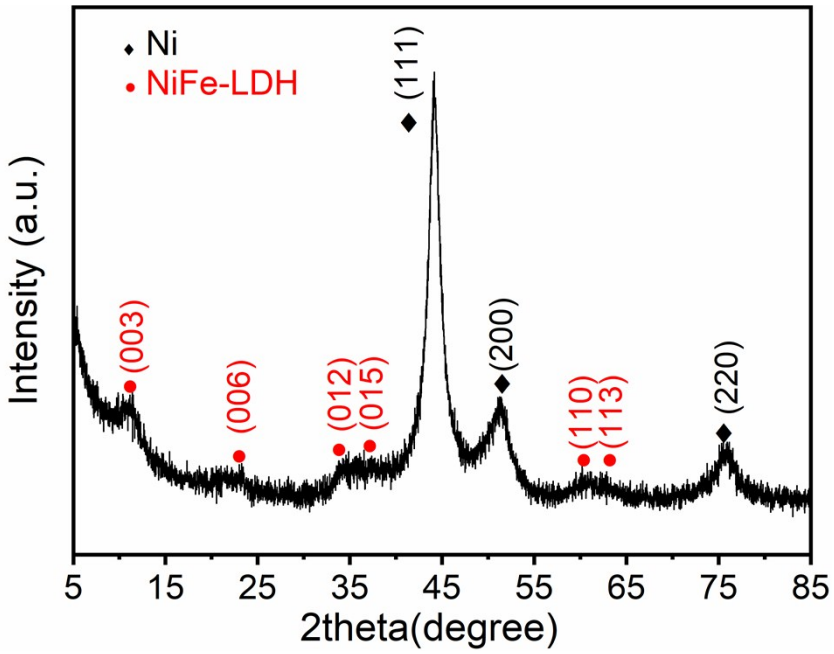

Supplementary Figure 14. XRD pattern of $Ni_{0.8}Fe_{0.2}$-AHNA after OER test.

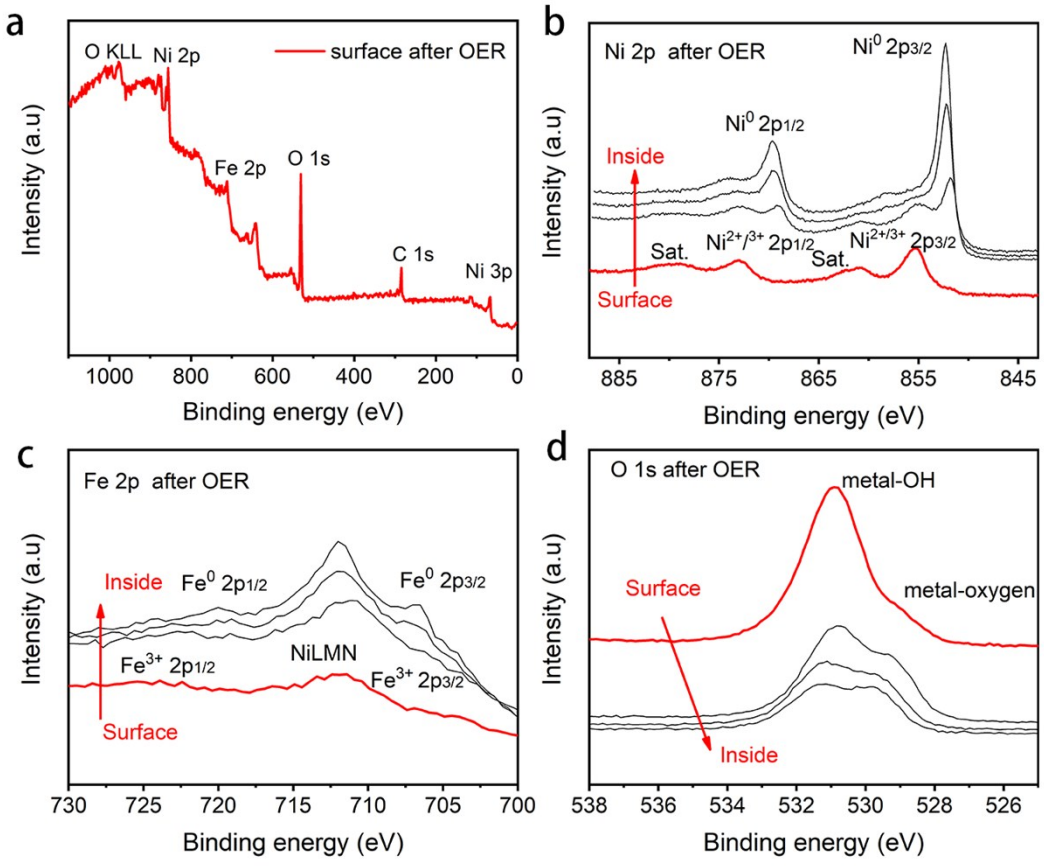

Supplementary Figure 15. XPS depth profile of $Ni_{0.8}Fe_{0.2}$-AHNA after OER. (a) Wide-scanning XPS spectra (surface). (b) Ni 2p XPS depth profile, (c) Fe 2p XPS depth profile and (d) O 1s XPS depth profile of the $Ni_{0.8}Fe_{0.2}$-AHNA after OER.

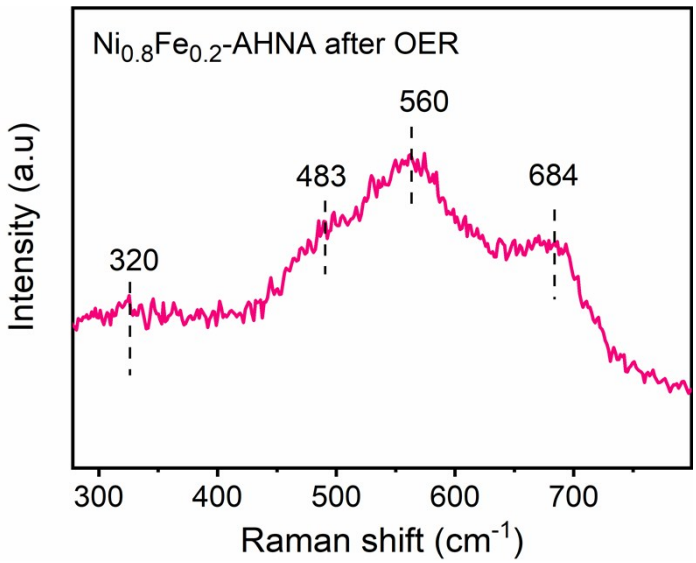

Supplementary Figure 16. Raman spectra of $Ni_{0.8}Fe_{0.2}$-AHNA after OER.

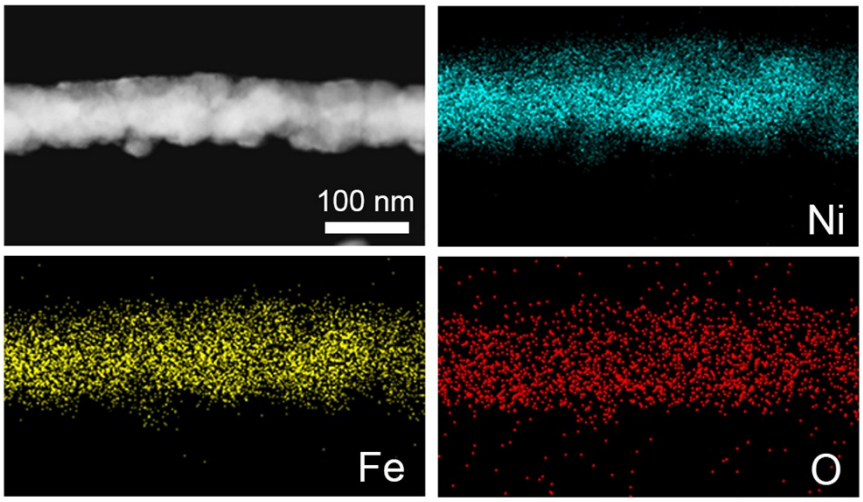

Supplementary Figure 17. EDX results of $Ni_{0.8}Fe_{0.2}$-AHNA after OER

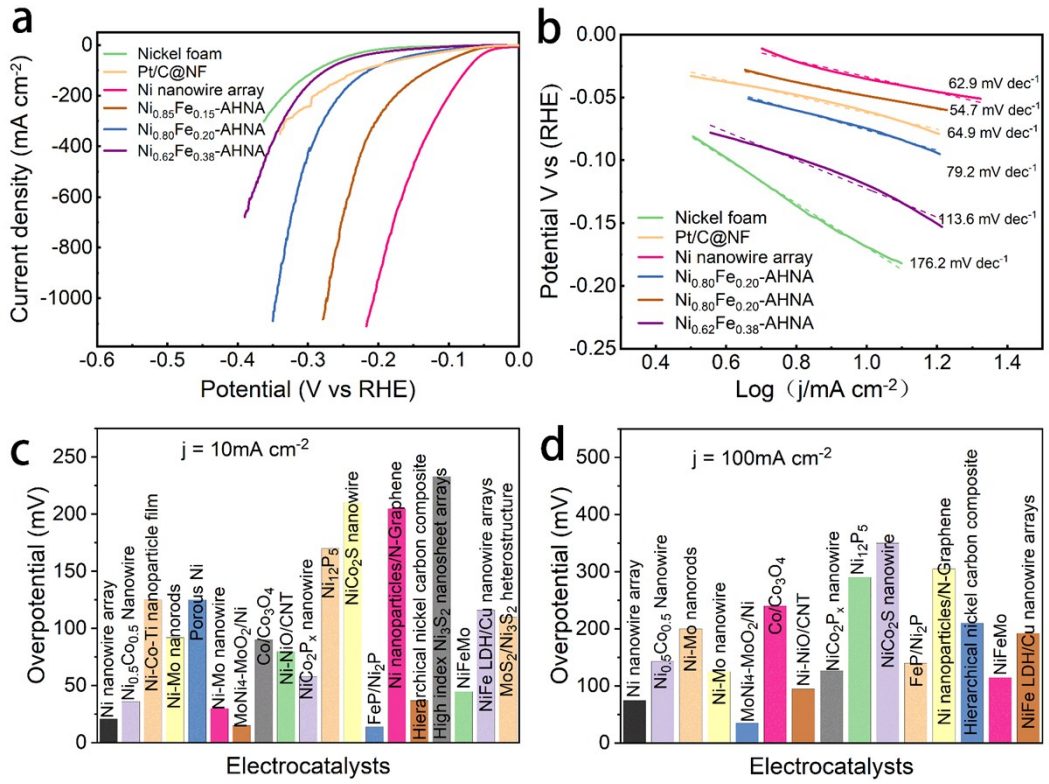

Supplementary Figure 18. Electrocatalytic Hydrogen evolution reaction. (a) The polarization curves recorded on different catalysts, (b) The corresponding Tafel plots, (c-d) Comparison of the overpotentials required at 10 and 100 mA cm^{-2} among our catalyst and available reported HER catalysts.

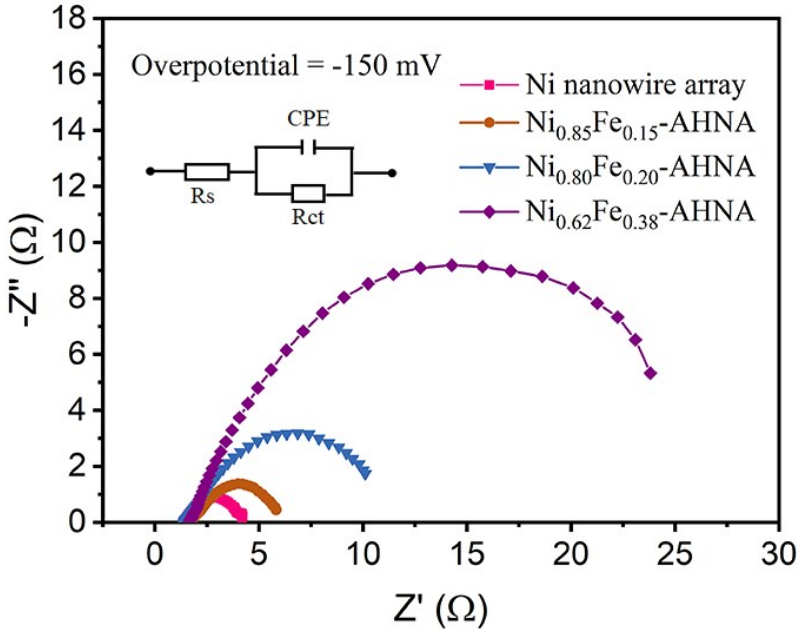

Supplementary Figure 19. EIS Nyquist plots of different Ni/Fe ratios Ni_xFe_{1-x}-AHNAs at the HER overpotential of 150mV.

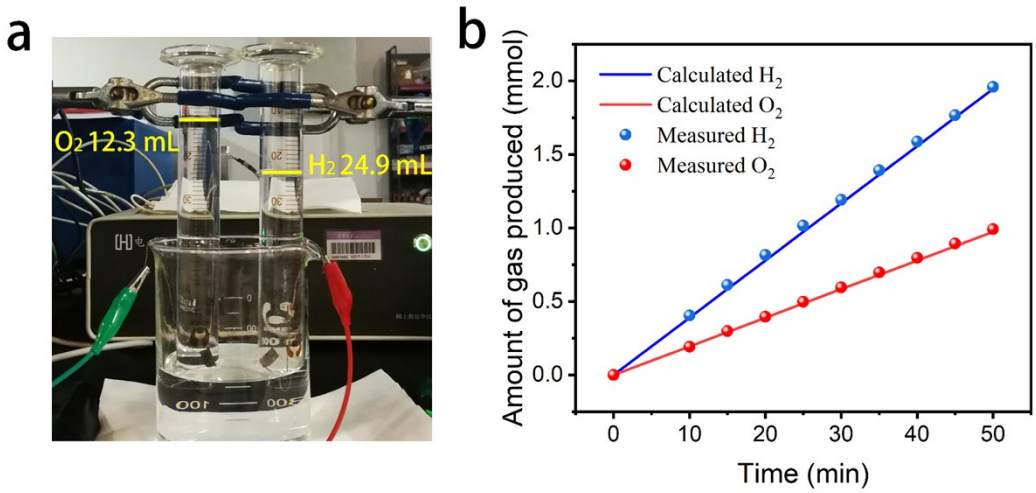

Supplementary Figure 20. (a) Digital photograph of H_2 and O_2 gas evolution on Ni nanowire array and $Ni_{0.8}Fe_{0.2}$-AHNA using water displacement method. (b) Experimental and theoretical amounts of H_2 and O_2 generated by the Ni nanowire array and $Ni_{0.8}Fe_{0.2}$-AHNA electrodes at a fixed current density of 500 mA cm^{-2}.

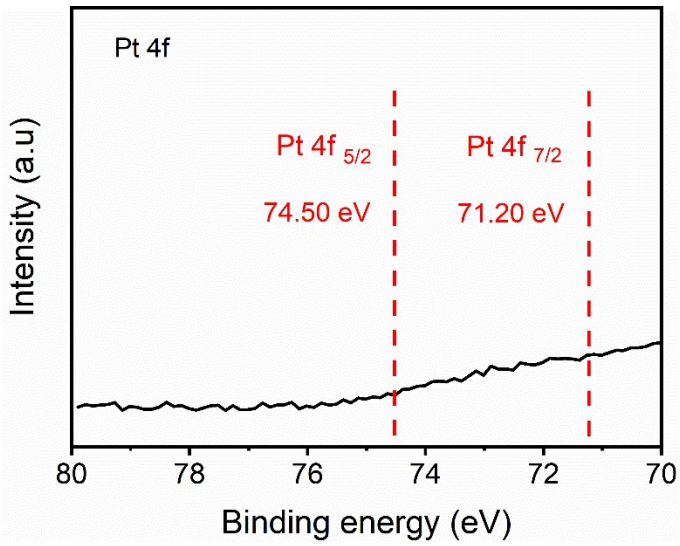

Supplementary Figure 21. Pt 4f XPS of Ni nanowire array, showing no obvious Pt signal on the surface of Ni nanowire.

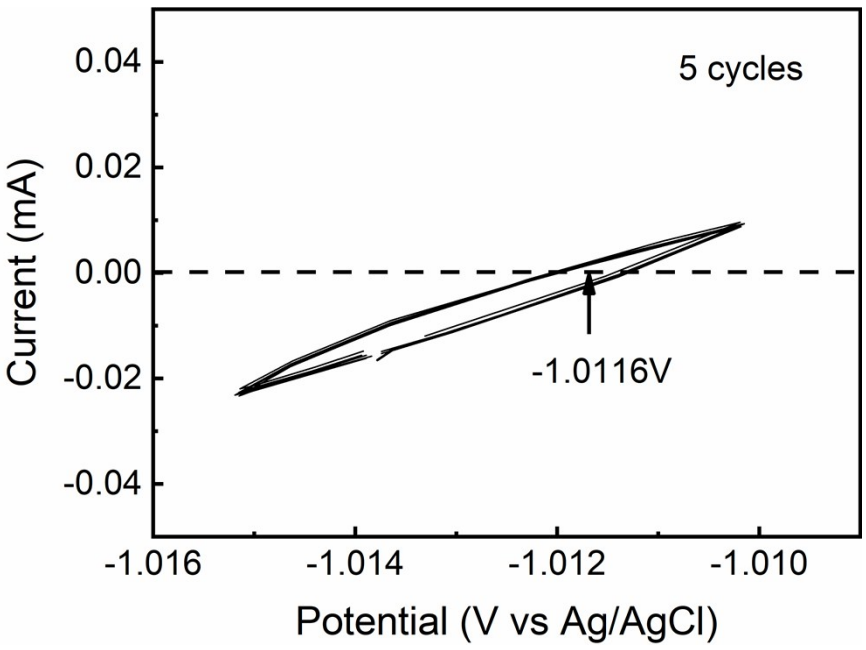

Supplementary Figure 22. Calibration of Ag/AgCl reference electrode with respect to RHE.

Supplementary Table 4. Comparison of the catalytic HER performance between our Ni nanowire array catalyst and robust earth-abundant electrocatalysts reported in 1 M KOH. η_{10} and η_{100} correspond to the current densities at the overpotentials of 10 and100 mV, respectively.

HER catalysts	Support	Mass loading(mg)	η_{10}(mA cm^{-2})	η_{100}(mA cm^{-2})	Tafel (mV dec^{-1})	Reference
Ni nanowire array	Ni foam	4.9	21	75	62.9	Our work
$Ni_{0.5}Co_{0.5}$ nanowire	none	7.5	36	143	34.1	Nano Energy, 2018, 51: 349-357.
Ni-Co-Ti nanoparticle film	Ni foam	4.5	125	NA	47	ACS Appl. Mater. Interfaces, 2017, 9(14): 12416-12426.
Ni-Mo nanorods on Ti mesh	Ni foam	0.68	92	200*	76	J. Mater. Chem. A, 2015, 3(40): 20056-20059.

Porous Ni	none	0.3	125	NA	81	Catal. Sci. Technol., 2017, 7(14): 3056-3064.
Ni-Mo nanowire	Ni foam	0.41	30	125*	86	Nano Energy, 2016, 27: 247-254.
$MoNi_4$-MoO_2/Ni	Ni foil	43.4	15	35	30	Nat. Commun., 2017, 8(1): 15437.
Co/Co_3O_4	Ni foam	0.85	90	240*	44	Nano Lett., 2015, 15(9): 6015-6021.
Ni/NiO-CNT	GCE	8	80	95*	51	Nat. Commun., 2014, 5(1): 4695.
$NiCo_2P_x$ nanowire	Ni foam	5.9	58	127*	34.3	Adv. Mater., 2017, 29(9): 1605502.
$Ni_{12}P_5$	Ni foam	NA	170	290*	NA	ACS Catal., 2016, 7(1): 103-109.
$NiCo_2S$ nanowire	Ni foam	NA	210	350*	58.9	Adv. Funct. Mater., 2016, 26(26): 4661-4672.
FeP/Ni_2P	Ni foam	8	14	140	24.2	Nat. Commun., 2018, 9(1):2551
Nickel Nanoparticles / Nitrogen-Doped Graphene	GCE	0.8	205	305*	160	Adv. Mater., 2017, 29(11): 1605957.
Hierarchical nickel–carbon composite	Fe foam	7.3±0.3	37	210*	57	Energy Environ. Sci., 2018, 11(9): 2363-2371.
High-Index Faceted Ni_3S_2 Nanosheet Arrays	Ni foam	1.6	223	NA	31	J. Am. Chem. Soc., 2015, 137(44): 14023-14026.
NiFeMo	Ni foam	1.6	45	115*	NA	ACS Energy Letters, 2018, 3(3): 546-554.
NiFe LDH/Cu nanowire arrays	Cu foam	NA	116	192	58.9	Energy Environ. Sci., 2017, 10(8): 1820-1827.
MoS_2/Ni_3S_2 Heterostructure	Ni foam	NA	110	NA	83.1	Angew. Chem. Int. Ed., 2016, 128(23): 6814-6819.

*** The value is calculated from the curves shown in the literature.**

Supplementary Table 5. Comparison of the overall-water-splitting activities among different earth-abundant electrocatalysts tested in 1 M KOH. V_{10}, V_{100} and V_{500} correspond to the cell voltages of the overall-water-splitting cell operated at 10, 100, and 500 mA cm^{-2}, respectively. $J_{1.7\ V}$ represents the current density at a cell voltage of 1.7 V.

Electrolyzers	V_{10}(V)	V_{100}(V)	V_{500}(V)	$J_{1.7V}$(mA cm^{-2})	Reference
Ni nanowire array$^{(-)}$//$Ni_{0.8}Fe_{0.2}$-AHNA$^{(+)}$	1.41	1.55	1.70	493	Our work
FeP/Ni_2P	1.42	1.60	1.71	406	Nat. Commun., 2018, 9(1):2551.
Porous MoO_2	1.53	1.8*	NA	67*	Adv. Mater., 2016, 28(19): 3785-3790.
NiFe LDH-NS@DG $^{(+)}$//NiFe LDH-NS@DG$^{(-)}$	NA	1.87*	1.67*	NA	Adv. Mater., 2016, 26(42): 7644-7651.
$Ni_{0.51}Fe_{0.49}P$ film	1.57	1.71*	NA	87*	Adv. Funct. Mater., 2016, 26(42): 7644-7651.
MoS_2/Ni_3S_2	1.56	1.71*	NA	91.4*	Angew. Chem. Int. Ed., 2016, 55(23): 6702-6707.
NiFe LDH/Cu NW	1.54	1.69*	NA	111*	Energy Environ. Sci., 2017, 10(8): 1820-1827.
$NiCo_2S_4$ nanowire array	1.63	2.097*	NA	16*	Adv. Funct. Mater., 2016, 26(26): 4661-4672.
EG/$Co_{0.85}$Se/NiFe-LDH	1.67	1.91*	NA	16.6*	Energy Environ. Sci., 2016, 9(2): 478-483.
NiP/Ni	1.61	2.102*	NA	24*	Adv. Funct. Mater., 2016, 26(19): 3314-3323.
NiFeOOH$^{(+)}$//$MoNi_4$$^{(-)}$	NA	1.49	1.59	NA	Energy Environ. Sci., 2018, 11(10): 2858-2864.
Co-B/Ni	1.41	1.87*	NA	28*	Adv. Energy Mater., 2018, 8(26): 1801372.
G-Pt_4Ni/GF//G-Ni_4Fe/GF	1.58	1.73*	NA	67*	Adv. Energy Mater., 2018, 30(26):

					1800403.
FeCoNi-hybrid nanotube arrays	1.429	1.72*	NA	90*	Nat. Commun., 2018, 9(1): 2452.

*** The value is calculated from the curves shown in the literature.**

References for ESI

1. C. Xu, Z. Li, C. Yang, P. Zou, B. Xie, Z. Lin, Z. Zhang, B. Li, F. Kang and C. P. Wong, *Adv Mater*, 2016, **28**, 4105-4110.
2. M. Kawamori, S. Yagi and E. Matsubara, *J. Electrochem. Soc.*, 2011, **158**.
3. M. B. Stevens, L. J. Enman, A. S. Batchellor, M. R. Cosby, A. E. Vise, C. D. M. Trang and S. W. Boettcher, *Chem. Mater.*, 2017, **29**, 120-140.
4. C. C. McCrory, S. Jung, J. C. Peters and T. F. Jaramillo, *J Am Chem Soc*, 2013, **135**, 16977-16987.
5. F.-F. Guo, Y. Wu, H. Chen, Y. Liu, l. yang, X. Ai and X. Zou, *Energy Environ. Sci.*, 2019, DOI: 10.1039/c8ee03405b.
6. L. C. Seitz, C. F. Dickens, K. Nishio, Y. Hikita, J. Montoya, A. Doyle, C. Kirk, A. Vojvodic, H. Y. Hwang and J. K. Norskov, *Science*, 2016, **353**, 1011-1014.
7. C. C. McCrory, S. Jung, I. M. Ferrer, S. M. Chatman, J. C. Peters and T. F. Jaramillo, *J Am Chem Soc*, 2015, **137**, 4347-4357.